RSC Advances

ROYAL SOCIETY OF CHEMISTRY

www.rsc.org/advances

Super toughed immiscible polycarbonate/poly(L-lactide) blend achieved by simultaneous addition of compatibilizer and carbon nanotubes

Yong-hong Wang, Xian-ling Xu, Jian Dai, Jing-hui Yang, Ting Huang, Nan Zhang, Yong Wang*, Zuo-wan Zhou, Ji-hong Zhang

Key Laboratory of Advanced Technologies of Materials (Ministry of Education), School of Materials Science & Engineering, Southwest Jiaotong University, Chengdu, 610031, China

Abstract: Polycarbonate/poly(L-lactide) (PC/PLLA) blend exhibits great potential application in many fields ranging from package, toy, electronic element and automobile, etc. However, the poor mechanical properties of the immiscible PC/PLLA blend restrict its application. In this work, a compatibilizer maleic anhydride grafted ethylene-octene copolymer (EOR-g-MAH) and functionalized carbon nanotubes (F-CNTs) were introduced into the immiscible PC/PLLA blend through simple melt-compounding processing. Mechanical property measurements showed that even if at low environmental temperature (0 ℃), the blend composites exhibited excellent fracture toughness, e.g. 40.9±2.1 kJ/m^2 at F-CNT content of 2 wt%. To better understand the toughening mechanism, the morphologies of the blend composites and the dispersion of F-CNTs and the rheological properties were systematically investigated. The results showed that with the combined effects of EOR-g-MAH and F-CNTs, the decreased PLLA particles were achieved. Most of F-CNTs selectively located in the PC matrix and some F-CNTs entered into PLLA particles. Specifically, at relatively high content (>2 wt%), F-CNTs formed percolated network structure. The toughening mechanism was then proposed based on the morphology evolution, the formation of F-CNT network structure and the impact-fractured surface morphologies. This work demonstrated that even if for the immiscible polymer blend, the super toughened blend composites could be achieved by the combined effects of compatibilizer and carbon nanotubes and therefore it provided an alternative strategy for largely improving the fracture toughness of immiscible polymer blends.

Keywords: PC/PLLA; Compatibilizer; Carbon nanotubes; Morphology; Toughening

* Corresponding author: Tel: +86 28 87603042;
E-mail: yongwang1976@163.com

1. Introduction

Polymer blending has been proved one of the most efficient ways to prepare new high-performance materials. To date, except only dozens of blends are completely miscible at the molecular level, most blends are immiscible. The mechanical properties of immiscible blends are determined by many factors, including morphology, crystalline structure and interfacial interaction between components, etc. Specifically, the appropriate interfacial interaction not only favors the dispersion of dispersed component but also favors the stress transferring between components under the load condition, which weakens the stress concentration phenomenon at the interface leading to the failure of the material. It is well known to all that compatibilizer, which can be introduced as the third component or can be formed through in-situ chemical reaction between components, has the role of reducing interfacial tension and improving interfacial interaction.[1,2]

Polycarbonate (PC) is a typical engineering plastic that exhibits good processing ability and excellent physical properties, including high tensile ductility, strength, heat deformation temperature (HDT) and electrical insulation. So far, PC-based articles have been widely used in the fields of package, toy, electronic element and automobile, etc. However, PC belongs to those engineering plastics, which exhibit high degree of dependence on petroleum resources. Therefore, developing new material from renewable sources to replace or partially replace PC satisfies the requirement of sustainable development and it has been a goal of high technological and environmental priority.

Poly(L-lactide) (PLLA) is a biocompatible and biodegradable polymer that can be obtained from completely renewable sources such as core, wheat and rice, and therefore it reduces the degree of dependence on petroleum sources. PLLA exhibits excellent tensile modulus and strength and it has been an alternative to replacing traditional petroleum-based engineering plastic. Therefore, introducing PLLA into other engineering plastic to develop new material attracts much attention of researchers. Different blends such as PLLA/polyamide (PA),[3-5] PLLA/poly(ethylene terephthalate) (PET),[6] PLLA/poly(butylene terephthalate) (PBT),[7] etc. have been developed in the last ten years.

Blending PC and PLLA to develop new material is very significant, because the addition of PLLA reduces the amount of PC in articles, which can weakens the dependence on the petroleum product. However, PC/PLLA blend is immiscible, and the blends usually exhibit deteriorated

mechanical properties compared with pure PC and/or PLLA due to the poor interfacial interaction between PC and PLLA.[8-11] Much effort has been put to improve mechanical properties of the blends. For example, Lee J. B. *et al.* [12] introduced different compatibilizers into PC/PLLA blends and found that the mechanical, morphological, rheological and degradation properties were greatly dependent upon the type of the compatibilizer. Kanzawa T. *et al.* [13] investigated the mechanical and morphological changes of the ternary PLLA/PC/poly(butylenes adipate-co-terephthalate) blends through reactive processing. The results showed that the tensile strain and impact strength of the ternary blends were considerably enhanced. Phuong V. T. *et al.* [14] introduced tetrabutylammonium tetraphenylborate (TBATPB) and triacetin into PC/PLLA blends through extrusion processing. The results showed that PC-PLLA copolymer was formed during the short extrusion time, and the compatibility between PC and PLLA was then improved.

However, from the results reported in the literatures one can see that for the traditionally compatibilized PC/PLLA blends, the degree of improvement of mechanical property is still very small, especially for the fracture resistance that usually determines the application of PC/PLLA articles under the impact load condition. Therefore, much work needs to be done to seek other strategies to further improve the fracture resistance of PC/PLLA blends. Recently, introducing functionalized carbon nanotubes (F-CNTs) into an immiscible polymer blends has been proved an efficient way to largely improve the fracture resistance of the blend.[15-19] The toughening efficiency is dependent on the selective location of F-CNTs in the blend composites. If F-CNTs selectively locate at the interface, the toughening mechanism is related to the bridge effect of F-CNTs at the blend interface that prevents the propagation of crack along the interface. As a consequence, largely enhanced tensile ductility can be achieved.[15-17] If F-CNTs selectively locate in one component of the blend, the toughening mechanism is proposed to be related to the formation of F-CNTs network structure that facilitates the stress transfer between components under the load condition.[18,19] In our previous work, F-CNTs were introduced into PC/PLLA (60/40, wt/wt) blend that exhibited cocontinuous morphology.[20] The results showed that the selective location of F-CNTs in PC component increased the phase size of PC component but decreased the phase size of PLLA component. Mechanical properties measurements showed that elongation at break and notched Izod impact strength were enhanced by adding a small amount of F-CNTs (0.5 wt%).

To further develop PC/PLLA material with high-performance, in the present work, we attempt to

simultaneously introduce compatibilizer, i.e. maleic anhydride grafted ethylene-octene copolymer (EOR-g-MAH), and F-CNTs into PC/PLLA blend. Interestingly, the new PC/PLLA/EOR-g-MAH/F-CNT material exhibits much higher impact strength but without apparent deterioration of modulus and tensile strength as compared with the binary PC/PLLA blend. Even if at low environmental temperature (0 ℃), the material also exhibits excellent impact strength. Namely, super toughened PC/PLLA blend composites are successfully achieved.

2. Experimental

2.1 Materials

PC (S-2001R, with a viscosity-average molecular weight (M_η) of 2.3 ×10^4 g/mol, a melt flow rate (MFR) of 7.5-10.5 g/10min (300 ℃/1.2 kg) and a density of 1.2 g/cm^3) was purchased from Mitsubishi Engineering-Plastics Corp. PLLA (2002D, with a D-isomer content of 4.3%, a weight-average molecular weight (M_w) of 2.53×10^5 g/mol, the MFR of 4-8 g/10min (190 ℃/2.16 kg) and the density of 1.24 g/cm^3) was purchased from NatureWorks®, USA. Functionalized carbon nanotubes (F-CNTs, containing 1.23 wt% carboxyl group) were obtained from Chengdu Institute of Organic Chemistry, Chinese Academy of Science (Chengdu, China). The outer diameters of F-CNTs were 20-30 nm, and the length of a single F-CNT was about 30 μm. Compatibilizer maleic anhydride grafted ethylene-octene copolymer (EOR-g-MAH) (KT-9, with MFR of 2.5 g/10min (190 ℃/2.16 kg)) was obtained from Shenyang Ketong Plastic Co., Ltd. The grafting ratio of MAH was 0.8 wt%.

2.2 Sample preparation

All materials were first dried at 70 ℃ for 10 h. A master batch of PC/F-CNT containing 10 wt% F-CNTs was prepared using a twin-screw extruder SHJ-30 (Nanjing Ruiya, China). Then the master batch was diluted by melt-blending with PC, EOR-g-MAH and PLLA to prepare the corresponding compositions. In this work, the weight ratio between PC and PLLA was maintained at 80:20, the content of EOR-g-MAH was maintained at 5 wt%, and the content of F-CNTs was varied from 0.5 to 5 wt%. The sample notation was defined as C8A2E5F*x*, where *x* represented the content of F-CNTs. For example, C8A2E5F2 indicated that the content of F-CNTs was 2 wt%. The melt blending was carried out at a screw speed of 100 rpm and melt temperatures of

170-200-220-240-255-255-250 ℃ from hopper to die. After being granulated, the pellets were injection-molded using an injection-molding machine EM80-V (Chen Hsong Machinery, China) to obtain the standard specimen. The melt temperatures were set at 240-255-255-250 ℃ from hopper to nozzle, and a mould temperature of 25 ℃ was used. The injection speed was 6.3 g/sec and the holding pressure was 35 MPa. For making a comparison, the binary PC/PLLA (80/20, C8A2) and the ternary PC/PLLA/EOR-g-MAH (80/20/5, C8A2E5) were also prepared through the completely same processing method.

2.3 Mechanical property measurement

Tensile properties were measured using a universal tensile machine AGS-J (SHIMADZU, China) according to ASTM D638. The dumbbell-shaped specimen had a width of 10 mm and a thickness of 4.2 mm. During the measurement, the gauge distance was set at 50 mm and a cross-head speed of 50 mm/min was used. For the notched Izod impact strength, it was measured using a rectangular sample with the width and thickness of 10 and 4.2 mm, respectively. The impact measurement was carried out at two different environmental temperatures, i.e. 23 and 0 ℃. The measurement was conducted on a XC-22Z impact tester (Chengde, China) according to ASTM D 256-04. The notch depth was 2.0 mm and the residual width of the specimen was about 8.0 mm. For each sample, the average value of mechanical properties reported was derived from the data of more than 5 specimens.

2.4 Scanning electron microscopy (SEM)

SEM was used to characterize sample morphology. Whether for the cryogenically fractured surface that obtained in the liquid nitrogen or for the impact-fractured surface that obtained during the impact measurement, the fractured surface was coated with a thin layer of gold before SEM characterization. To further clarify the dispersion of EOR-g-MAH, the cryogenically fractured surface of the C8A2E5 sample was further treated using *n*-heptane at 50 ℃ for 4 h to remove EOR-g-MAH component. Then, the treated surface was carefully washed and coated before SEM characterization. The characterization was conducted on a Fei Inspect (FEI, the Netherlands), and an accelerating voltage of 5.0 kV was used.

2.5 Transmission electron microscopy (TEM)

TEM was further used to characterize the morphology of composition and the dispersion of F-CNTs in the material. The characterization was conducted on a Tecnai G2 F20 (FEI, USA), and

an operating voltage of 200 kV was used. An ultrathin section with a thickness of about 90 nm, which was cut using a cryo-diamond knife on a microtome EM UC6/F6 (LEICA, Germany), was used. Before TEM characterization, the samples containing EOR-g-MAH were stained with OsO_4.

2.6 Rheological measurement

The rheological measurement was conducted on a stress-controlled rheometer AR 2000ex (TA Instruments, USA). The sample disk was first prepared through a compression-molding method that was carried out at melt temperature of 250 ℃ and pressure of 5 MPa. The sample had a thickness of 1.0 mm and a diameter of 20 mm. During the rheological measurement process, the frequency sweep from 0.01 to 100 Hz was performed at 250 ℃ under dry nitrogen atmosphere. For all the measurements, the samples were tested within the linear viscoelastic strain range, which could be estimated by an initial survey through a dynamic strain sweep experiment at strains ranging from 0.01 to 100%.

3. Results and discussion

3.1 Mechanical properties

Figure 1 shows the typical engineering stress-strain curves of the PC/PLLA/EOR-g-MAH/F-CNT specimens and the corresponding tensile properties. For making a comparison, the results of the binary PC/PLLA and the ternary PC/PLLA/EOR-g-MAH specimens are also shown. It is worth noting that PC is a ductile polymer with apparent yielding and cold-drawing behaviors while PLLA is a brittle polymer without yielding during the universal tensile process. From Fig. 1 one can see that the binary PC/PLLA (80/20) specimen exhibits the elongation at break of 102.2±1.9%. It has already been proved that addition of a small amount of PLLA can slightly enhance the tensile ductility of PC, which can be attributed to the toughening effect of rigid PLLA particles on ductile PC matrix.[9,14] In our previous work, 30 wt% PLLA was introduced into PC and the elongation at break was increased from 83.8% of pure PC to 119.6% of the PC/PLLA (70/30) specimen.[9] Similar results were also reported by Phuong V. T. *et al.*[14] In their work, the PC/PLLA (70/30) specimen exhibited elongation at break of about 125±3.3%, much higher than that of pure PC (84.4±4.3%). In the present work, although the composition is different, the binary PC/PLLA specimen still exhibits the enhanced tensile ductility as compared with pure PC, which further proves the weak toughening effect of PLLA on PC. For the ternary

PC/PLLA/EOR-g-MAH specimen, the elongation at break is increased up to 132.4±0.7%. This proves that EOR-g-MAH is a compatibilizer of immiscible PC/PLLA blend, and it has a role of improving the tensile ductility of the material.[12] Although the presence of EOR-g-MAH induces the deterioration of tensile modulus, the addition of F-CNTs apparently enhances the tensile modulus of specimen. Specifically, the tensile modulus of specimen increases gradually with increasing F-CNT content. However, from Fig. 1 one can also see that addition of high content of F-CNT induces the dramatic deterioration of tensile ductility of specimen. For example, the elongation at break is dramatically decreased from 132.4±0.7% of the C8A2E5 specimen to 28.8 ±3.9% of the C8A2E5F5 specimen. There are at least two possibilities that take charge of the deterioration of the tensile ductility. One possibility is related to the formation of large F-CNT agglomerates that act as the stress concentrator, which results in the failure of the sample during the tensile process. The other possibility is related to the formation of dense F-CNT network structure in the material, which prevents the plastic flow of PC macromolecules along the tensile direction. The formation of F-CNT network structure will be proved in the next section through rheological measurement.

The impact strength of sample was first measured at room temperature (23 ℃). The C8A2 specimen exhibits impact strength of 12.9±0.6 kJ/m^2. Although the value is higher than that of pure PLLA (3.1±0.1 kJ/m^2), it is much smaller than that of pure PC sample (66.9±2.7 kJ/m^2). This proves the poor interfacial interaction between components in the binary blend. Addition of a small amount of EOR-g-MAH, the impact strength of the ternary blend specimen is greatly enhanced to 73.5±5.7 kJ/m^2, which is nearly 6 times higher than that of the binary blend specimen. Further enhanced fracture resistance is achieved for the C8A2E5F0.5 specimen and the impact strength is increased up to 87.1±3.0 kJ/m^2. Furthermore, it is interesting to observe that the specimen was not completely fractured during the impact measurement. As shown in Figure 2, nearly half of the specimen was not fractured. The similar phenomenon is also observed for other samples containing high content of F-CNTs. It is well known to all that during the Charpy test, the break of the specimen is essential; otherwise the results of the Charpy test are meaningless. Therefore, to clearly understand the variation of the fracture resistance of specimen, the impact measurement was further carried out at low environmental temperature, i.e. 0 ℃. In this condition, nearly all the specimens were completely fractured during the impact measurement.

As shown in Figure 3, the C8A2 and C8A2E5 specimens exhibit the impact strength of 7.3±0.6 and 27.5±1.5 kJ/m^2, respectively. However, it is worth noting that the toughening efficiency of EOR-g-MAH at low environmental temperature is slightly decreased compared with that measured at room temperature. Here, the impact strength of the C8A2E5 is only about 4 times higher than that of the C8A2 specimen. Surprisingly, the impact strength of the PC/PLLA/EOR-g-MAH/F-CNT specimen increases gradually with increasing content of F-CNTs until very high content of F-CNTs are present in the material. For example, the C8A2E5F0.5 specimen exhibits the impact strength of 31.6±1.1 kJ/m^2. For the C8A2E5F1 and C8A2E5F2 specimens, the impact strength is increased up to 35.8±0.9 and 40.9±2.1 kJ/m^2, respectively. Specifically, it is still observed that the C8A2E5F2 specimen was not completely fractured. In a word, with simultaneous addition of compatibilizer and carbon nanotubes, super toughened PC/PLLA blend composites are successfully achieved.

Analyzing the impact-fractured surface morphology facilitates to further understand the fracture behavior of specimen. Here, the fractured surfaces of representative specimens, which were obtained at 0 ℃, were characterized using SEM. Figure 4 shows the surface morphologies characterized at relatively small magnification. It can be seen that although the specimen is not completely fractured, the impact-fractured surface in the fractured part of the C8A2 specimen is very smooth, which indicates that the fracture process occurs at relatively high speed. Obviously, the C8A2 specimen exhibits the typical brittle fracture mode. This agrees well with its low impact strength (7.3±0.6 kJ/m^2) as shown in Fig. 3. Different from the smooth surface of the C8A2 specimen, the C8A2E5 specimen exhibits coarse surface, indicating that the fracture resistance of the specimen is enhanced. Adding F-CNTs into the material further enhances the roughness of the fractured surface. Specifically, one can see that a part of sample is pulled out from the fractured surface. Such phenomenon becomes more apparent at relatively high F-CNT content. For the C8A2E5F2 specimen, even at low magnification, one can also see the intense plastic deformation of specimen.

More differences in surface morphologies of different specimens can be clearly seen from the SEM images obtained at high magnifications. Generally speaking, the fracture of a specimen during the impact process experiences two stages, crack initiation and crack propagation. Correspondingly, the fractured surface can be divided into crack initiation zone (Zone A as shown

in Fig. 4a) and crack propagation zone (zone B and C as shown in Fig. 4a, representing the early stage and later stage of crack propagation, respectively). Therefore, the surface morphologies in different zones were carefully characterized at high magnification. As shown in Figure 5, for the C8A2 specimen (Fig. 5a), in all zones (Zones A-C), one can see that some PLLA particles are debonded from PC matrix, proving the weak interfacial interaction between PC and PLLA. For the C8A2E5 specimen (Fig. 5b), even in the crack initiation zone (Zone A), one can observe the plastic deformation of specimen. The plastic deformation becomes more apparent in the specimens containing F-CNTs (Figs. 5c and 5d). Specifically, besides the plastic deformation of PC matrix, the fibrillated PLLA component is also observed in the crack initiation zone of the C8A2E5F2 specimen (Zone A). In the later stage of crack propagation process (Zone C), it is difficult to differentiate PLLA component from PC matrix, and the specimen exhibits very intense plastic deformation. This means that the plastic deformation of PC matrix is companioned with the simultaneous plastic deformation of PLLA component. It is well known to all that PLLA is a typical brittle material and pure PLLA usually exhibits the brittle fracture mode without any plastic deformation. Generally speaking, the fibrillation of material is greatly related to the intense plastic deformation occurred under the load condition.[21] This indicates that in the present work, the plastic deformation of PLLA component is also activated with the combined effects of EOR-g-MAH and F-CNTs. The fibrillar PLLA observed during the impact measurement has also been reported elsewhere and it is believed one of the main reasons for the largely enhanced fracture resistance.[20,22] However, it is still not clear why the brittle PLLA component can be fibrillated or deformed. In the next section, we will attempt to explain the mechanism for the fibrillation of PLLA component.

3.2 Morphology

The mechanical properties of the blend composites are mainly related to their microstructure and morphology, including the crystalline structure of components, the dispersed particle morphology and the dispersion of fillers. In the present work, PC is an amorphous polymer and no crystallization occurs during the whole melt-processing procedures. PLLA is a typical semicrystalline polymer, however, it is still in the amorphous state through the traditional melt-processing due to that the crystallization ability of PLLA is very small and the relative high cooling rate prevents the crystallization of PLLA. Even if with the presence of F-CNTs, which

usually exhibit excellent nucleation effect for crystallization of semicrystalline polymer, the crystallization of PLLA is still very difficult and no crystallization occurs during the whole melt-processing procedures.[20] Therefore, the influence of crystalline structure change on the mechanical properties of the PC/PLLA/EOR-g-MAH/F-CNT can be ignored. So, the main attention is focused on the morphological change of the blend and the selective location of F-CNTs in the blend composites.

Here, the morphology of the blend composites and the dispersion of F-CNTs were characterized using SEM and TEM. Figure 6 exhibits the SEM images of samples. For the binary PC/PLLA blend (Fig. 6a), it exhibits the typical "two-phase structure" feature, proving the weak interfacial interaction between PC and PLLA. With the addition of EOR-g-MAH (Fig. 6b), although the blend still shows the "two-phase structure" feature, one can see that some EOR-g-MAH locates at the interface between PC and PLLA. The dispersion of EOR-g-MAH can be further proved by the image shown in Fig. 6f, in which only EOR-g-MAH was first removed by *n*-heptane and the black holes represent the EOR-g-MAH component. This indicates that the selectively located EOR-g-MAH can exhibit the bridge effect to strengthen the interaction between PC and PLLA. On the other hand, different from the smooth surface of the C8A2 sample, the cryogenically fractured surface of the C8A2E5 sample becomes rougher. For the PC/PLLA/EOR-g-MAH/F-CNT blend composites, although the C8A2E5F0.5 sample (Fig. 6c) exhibits the similar morphology to that of the C8A2E5 sample, apparently decreased PLLA particles are observed in the sample containing high content of F-CNTs, especially in the C8A2E5F5 sample (Fig. 6e). The decrease of PLLA particle size can be ascribed to the increase of the melt viscosity induced by high content of F-CNTs that prevent the migration of dispersed PLLA particles and the steric hindrance effect of F-CNTs that prevents the collision and aggregation of adjacent PLLA particles.[23-25] The variation of viscosity of samples can be seen in the following section.

Figure 7 exhibits the TEM images of the representative samples. Because of the inherent electron density difference between PC and PLLA, the "two-phase structure" feature can also be clearly seen: PC component appears dark while PLLA component appears white in the image. Similar phenomenon in appearance has been reported elsewhere.[14] EOR-g-MAH can be also differentiated since it can be stained by OsO_4. Specifically, from Fig. 7c and 7d one can see that most of F-CNTs

are selectively located in the PC matrix, and some of F-CNTs penetrate PLLA particles or a part of a single F-CNT enter into PLLA particles. Obviously, these F-CNTs can also exhibit the bridge effect to intensify the interaction between PC and PLLA, facilitating the stress transfer in the material and avoiding the stress concentration at the blend interface under the load condition.[17] Furthermore, from Fig. 7d one can also see that some F-CNTs contact each other and form the network-like structure in the PC matrix. This also indicates that stress can transfer along the osculatory F-CNTs. In other word, the F-CNT network also avoids the presence of stress concentration in the PC matrix, which facilitates the improvement of the fracture resistance of the sample.

3.3 Rheological properties

The formation of F-CNT network structure in the material can be further proved through rheological measurement, because rheological measurement provides not only a fundamental understanding of the nature of the processability and the structure–property relationship of the composites but also the information about the dispersion and microstructure of nanofiller in the polymer melt. Figure 8 exhibits the storage modulus (G'), loss modulus (G''), Cole-Cole plots of G' versus G'' and complex viscosity (η^*). From Fig. 8a one can see that the presence of EOR-g-MAH induces the slight increase of G' at low frequencies. Similar phenomena have been widely reported in literatures.[26-29] To date, many researches have shown that the interfacial activity and micelle formation greatly influence the rheological behaviors of the compatibilized blends. For example, Entezam M. *et al.* [30] proved that micelle formation due to extra amounts of compatibilizer in a system with higher interfacial activity resulted in an increase of the elastic modulus. Specifically, they concluded that the solid like rheological behavior was attributed to the interconnectivity between dispersed phase domains through matrix polymer chains trapped by the compatibilizer shell. For the PC/PLLA/EOR-g-MAH/F-CNT blend composites, the presence of a small amount (0.5 wt%) of F-CNTs does not induce the apparent change of G' at all frequencies. However, further increasing the content of F-CNTs induces the great increase of G' at low frequencies. Specifically, at F-CNT content of 2 and 5 wt%, the storage modulus curve even presents a platform at low frequencies. This indicates that G' keeps invariant and the melt exhibits apparent solid-like response. Now, it has been widely accepted that for the composites

filled with nanofillers, the presence of the platform in the storage modulus curve at low frequency is related to the formation of a percolated nanofiller network structure in the melt.[31-33] Therefore, from Fig. 8a one can believe that the percolated F-CNT network structure forms in the PC/PLLA/EOR-g-MAH/F-CNT blend composites with high content of F-CNTs. The similar variation trends are also observed for G'' (Fig. 8b). Although the platform at low frequencies becomes inconspicuous, the increase of G'' with increasing content of F-CNTs also proves an enhancement of molecular interactions, namely the molecular mobility becomes more difficult.

Fig. 8c shows the Cole-Cole plots of G' versus G''. It can be seen that the C8A2 sample exhibits an approximate linear relationship between G' and G''. The presence of F-CNTs induces the deviation from the linear relationship, especially when high content of F-CNTs are present in the melt. It has been reported elsewhere that the change in the slope of the Cole-Cole plots indicate the significant change in microstructure of the melt. When the Cole-Cole plots exhibit the deviation from the linear relationship between G' and G'', the nanofiller forms the percolated rheological network structure in the melt.[34,35] Therefore, Fig. 8c also proves the formation of the percolated F-CNT network structure in the PC/PLLA/EOR-g-MAH/F-CNT blend composites with high content of F-CNTs.

The variation of η^* with increasing content of F-CNTs is shown in Fig. 8d. For making a comparison, the viscosity of pure PC and PLLA is also shown in the inserted graph. From the inserted graph one can see that in all frequencies, the melt viscosity of pure PC is much higher than that of the pure PLLA and the viscosity ratio between PC and PLLA component is bigger than 10. Furthermore, it can be seen that either for the C8A2 sample or for the C8A2E5 sample, it exhibits the Newtonian plateau with nearly invariant η^* at relatively low frequencies. However, the presence of F-CNTs induces the enhancement of η^*, especially at low frequencies. The more the F-CNTs in the blend composites, the more apparent the enhancement of η^* is. Obviously, the molecular mobility of the melt is greatly restricted by F-CNTs. Previous morphological characterization has shown that most of F-CNTs are present in the PC component. Therefore, it can be concluded that the viscosity ratio between PC and PLLA component in the blend composites is also increased. This is possibly the other reason for the decrease of PLLA particle

size as shown in Fig. 6. In addition, it can be seen that F-CNTs induce the change of the melt from the Newtonian fluid to the non-Newtonian fluid, and the feature of shear thinning behavior becomes more apparent at high content of F-CNTs.

3.4 Further understanding about the toughening mechanism

To further understand the fracture behavior and toughening mechanism of the PC/PLLA/EOR-g-MAH/F-CNT blend composites, the plastic deformation behavior from a broken Izod sample was further characterized using TEM. The schematic representation showing the sampling method from a broken Izod sample (cross-section of a broken sample in a plane perpendicular to the fractured surface) and the corresponding TEM image are shown in Figure 9. From Fig. 9b one can see that even if underneath the fractured surface, the rigid PLLA particles are also deformed. Furthermore, besides the deformation of rigid PLLA particles, which is also observed from the impact-fractured surface morphologies as shown in Fig. 5, one can also see the orientation of F-CNTs in the similar direction to that of the deformed PLLA particles. It has been proved that the motion and orientation of nanofiller during the fracture process of sample facilitate the energy dissipation, which results in the improvement of fracture toughness.[36] Considering the relatively bigger modulus of PLLA as compared with the ductile PC matrix, it can be believed that the orientation of F-CNTs and the deformation of PLLA particles are mainly attributed to the plastic deformation of PC matrix under the load condition. Therefore, the toughening mechanism of the PC/PLLA/EOR-g-MAH/F-CNT blend composites is proposed as follows.

To better understand the toughening mechanism, more visualized schematic representations are shown in Figure 10. Fig. 10a represents the dispersion of PLLA particles and F-CNTs in the sample as prepared. Previous TEM images (Fig. 7) have proven that at relatively high content, some of F-CNTs penetrate PLLA particles or a part of a single F-CNT enter into PLLA particles. Obviously, these F-CNTs can exhibit the bridge effect to intensify the interfacial adhesion between PC and PLLA. Under the load condition (Fig. 10b), the dispersed PLLA particles act as the stress concentrator. With the aid of F-CNTs, the local stress formed around PLLA particles can be easily transferred to PC matrix (as shown by arrows), especially when F-CNTs form the network structure. In this condition, the plastic deformation of PC matrix is promoted. With the increase of plastic deformation degree of PC matrix, the coiled F-CNTs agglomerates are disentangled and oriented along the deformation direction of PC matrix (Fig. 10c), leading to more energy

dissipation. Simultaneously, under the hydrostatic stress of around PC matrix and the inducing effect of oriented F-CNTs, the deformation of rigid PLLA particles is also promoted. This also facilitates the energy absorption of sample during the impact fracture process. Obviously, the more the F-CNTs in the blend composites, the denser the F-CNTs network structure, and the more apparent the bride effect of F-CNTs is, and therefore the more energy dissipation during the impact process are. However, it is worth noting that very high content of F-CNTs (5 wt%) result in the formation of large F-CNTs agglomerates on the one hand, which act as the stress concentrator under the load condition. On the other hand, too dense F-CNT network can deteriorate the plastic deformation of PC matrix through restricting the motion of PC chain segments. That is the reason why the C8A2E5F5 sample exhibits the deteriorated tensile ductility and impact fracture toughness as compared with the blend composites containing relatively smaller F-CNTs ($\leq$ 2 wt%).

4. Conclusions

In summary, the PC/PLLA/EOR-g-MAH/F-CNT blend composites have been prepared through melt-compounding processing. The mechanical properties measurements show that F-CNTs do not apparently change the tensile properties of the blend composites. However, largely enhanced impact strength is observed for the PC/PLLA/EOR-g-MAH/F-CNT blend composites even if the measurement is carried out at relatively low environmental temperature (0 ℃) and the impact strength increases gradually with increasing content of F-CNTs until very high content of F-CNTs are present in the blend composites, which induces the deterioration of the fracture resistance. Besides the plastic deformation of PC matrix, the plastic deformation of rigid PLLA particles and the orientation of F-CNTs are also observed. With the combined effects of EOR-g-MAH and F-CNTs, the decreased PLLA particles are achieved. Most of F-CNTs are observed in the PC matrix and form the percolated network structure, which has been further proved by rheological measurement. It is proposed that the largely improved fracture toughness is mainly attributed to the compatibilizing effect of EOR-g-MAH, which greatly improves the interfacial interaction between PC and PLLA components, and the formation of F-CNT network structure and the bridge effect of F-CNTs that penetrate PLLA particles, which not only facilitate the stress transfer in the material but also promote the orientation of F-CNTs and the plastic deformation of rigid PLLA

particles, leading to more energy dissipation during the fracture process.

Conflict of interest

The authors declare no competing financial interests.

Acknowledgement

Authors express their sincere thanks to the National Natural Science Foundation of China (51473137 and 50973090).

References

1. C. Koning, M. V. Duin, C. Pagnoulle and R. Jerome. *Prog. Polym. Sci.*, 1998, **23**, 707–757.
2. N. C. Liu and W. E. Baker, *Adv. Polym. Technol.*, 1992, **11**, 249–262.
3. R. Khankrua, S. Pivsa-Art, H. Hiroyuki and S. Suttiruengwong, *Polym. Degrad. Stabil.*, 2014, **108**, 232–240.
4. G. Stoclet, R. Seguela and J. M. Lefebvre, *Polymer*, 2011, **52**, 1417–1425.
5. R. Patel, D. A. Ruehle, J. R. Dorgan, P. Halley and D. Martin, *Polym. Eng. Sci.*, 2014, **54**, 1523–1532.
6. F. P. La Mantia, L. Botta, M. Morreale and R. Scaffaro, *Polym. Degrad. Stabil.*, 2012, **97**, 21–24.
7. M. L. Di Lorenzo, P. Rubino and M. Cocca, *J. Appl. Polym. Sci.*, 2014, **131**, 40372.
8. C. Liu, S. Lin, C. Zhou and W. Yu, *Polymer*, 2013, **54**, 310–319.
9. Y. H. Wang, Y. Y. Shi, J. H. Yang, T. Huang, N. Zhang and Y. Wang, *J. Appl. Polym. Sci.*, 2013, **127**, 3333–3339.
10. A. M. Harris and E. C. Lee, *J. Appl. Polym. Sci.*, 2013, **128**, 2136–2144.
11. Y. Wang, S. M. Chiao, T. F. Hung and S. Y. Yang, *J. Appl. Polym. Sci.*, 2012, **125**, E402–E412.
12. J. B. Lee, Y. K. Lee, G. D. Choi, S. W. Na, T. S. Park and W. N. Kim, *Polym. Degrad. Stabil.*, 2011, **96**, 553–560.
13. T. Kanzawa and K. Tokumitsu, *J. Appl. Polym. Sci.*, 2011, **121**, 2908–2918.
14. V. T. Phuong, M. B. Coltelli, P. Cinelli, M. Cifelli, S. Verstichel and A. Lazzeri, *Polymer*, 2014, **55**, 4498–4513.

15. F. M. Xiang, J. Wu, L. Liu, T. Huang, Y. Wang,C. Chen, Y. Peng, C. X. Jiang, Z. W. Zhou, *Polym. Adv. Technol.*, 2011, **22**, 2533–2542.
16. Y. Y. Shi, Y. L. Li, F. M. Xiang, T. Huang, C. Chen,Y. Peng, Y. Wang, *Polym. Adv. Technol.*, 2012, **23**, 783–790.
17. J. Chen, Y. Y. Shi, J. H. Yang, N. Zhang, T. Huang, Y. Wang, *Polymer*, 2013, **54**, 464–471.
18. L. Liu, Y. Wang, Y. L. Li, J. Wu, Z. W. Zhou, C. X. Jiang, *Polymer*, 2009, **50**, 3072–3078.
19. Y. Y. Shi, W. B. Zhang, J. H. Yang, T. Huang, N. Zhang, Y. Wang, G. P. Yuan, C. L. Zhang, *RSC Adv.*, 2013, **3**, 26271–26282.
20. Y. H. Wang, Y. Y. Shi, J. Dai, J. H. Yang, T. Huang, N. Zhang, Y. Peng and Y. Wang, *Polym. Int.*, 2013, **62**, 957–965.
21. R. S. Hadal, A. Dasari, J. Rohrmann and R. D. K. Misra, *Mater. Sci. Eng. A*, 2004, **372**, 296–315.
22. S. D. Park, M. Todo, K. Arakawa and M. Koganemaru, *Polymer*, 2006, **47**, 1357–1363.
23. D. F. Wu, D. Lin, J. Zhang, W. Zhou, M. Zhang, Y. Zhang, D. Wang and B. Lin, *Macromol. Chem. Phys.*, 2011, **212**, 613–626.
24. F. F. Tao, D. Auhl, A. C. Baudouin, F. J. Stadler and C. Bailly, *Macromol. Chem. Phys.*, 2013, **214**, 350–360.
25. A. C. Baudouin, D. Auhl, F. F. Tao, J. Devaux and C. Bailly, *Polymer*, 2011, **52**, 149–156.
26. A. Ajji, L. A. Utracki, *Polym. Eng. Sci.*, 1996, **36**, 1574–1585.
27. W. Gleinser, H. Braun, C. Friedrich, H. J. Cantow, *Polymer*, 1994, **35**, 128–135.
28. M. Iza, M. Bousmina, R. Jerome, *Rheol. Acta*, 2001, **40**, 10–22.
29. C. Sailer, U. A. Handge, *Macromolecules*, 2007, **40**, 2019–2028.
30. M. Entezam, H. A. Khonakdar, A. A. Yousefi, S. H. Jafari, U. Wagenknecht, G. Heinrich, B. Kretzschmar, *Macromol. Mater. Eng.*, 2012, **297**, 312–328.
31. R. Krishnamoorti and E. P. Giannelis, Macromolecules, 1997, 30, 4097–4102.
32. P. Pötschke, T. D. Fornes and D. R. Paul, Polymer, 2002, 43, 3247–3255.
33. Z. H. Xu, Y. H. Niu, L. Yang, W. Y. Xie, H. Li, Z. H. Gan and Z. G. Wang, *Polymer*, 2010, **51**, 730–737.
34. R. A. Khare, A. R. Bhattacharyya, A. R. Kulkarni, M. Saroop and A. Biswas, *J. Polym. Sci. Part B: Polym. Phys.*, 2008, **46**, 2286–2295.

35. H. K. F. Cheng, N. G. Sahoo, Y. Z. Pan, S. H. Chan, J. H. Zhao and G. Chen, *J. Polym. Sci. Part B: Polym. Phys.*, 2010, **48**, 1203–1212.

36. T. H. Zhou, W. H. Ruan, M. Z. Rong, M. Q. Zhang and Y. L. Mai, *Adv. Mater.* 2007, **19**, 2667–2671.

Figure captions:

Figure 1: (a) Typical engineering stress-strain curves of specimens and (b) the corresponding tensile properties.

Figure 2: (a) Optical photograph of impact-fractured C8A2E5F2 sample and (b) the corresponding SEM image of impact-fractured surface morphology obtained at low magnification.

Figure 3: Notch Izod impact strength of samples as indicated in the graph. The measurement was carried out at low environmental temperature (0 ℃).

Figure 4: SEM images showing the impact-fractured surface morphologies of representative samples obtained at low magnification. (a) C8A2, (b) C8A2E5, (c) C8A2E5F0.5 and (d) C8A2E5F2

Figure 5: SEM images showing the impact-fractured surface morphologies at different zones as shown in Figure 4a. The images were taken at high magnification. (a) C8A2, (b) C8A2E5, (c) C8A2E5F0.5 and (d) C8A2E5F2

Figure 6: (a-e) SEM images showing the cryogenically fractured surface morphologies of different samples and (f) Morphology of the representative C8A2E5 sample when EOR-g-MAH was removed by *n*-heptane. (a) C8A2, (b) C8A2E5, (c) C8A2E5F0.5, (d) C8A2E5F2 and (e) C8A2E5F5

Figure 7: TEM images showing the morphologies of PLLA component and the dispersion of F-CNTs in different samples. (a) C8A2, (b) C8A2E5, (c) C8A2E5F0.5 and (d) C8A2E5F2

Figure 8: Rheological properties of different samples as indicated in the graphs. The inserted graph shows the comparison of viscosity between pure PC and PLLA. (a) Storage modulus, (b) loss modulus, (c) Cole-Cole plots of storage modulus versus loss modulus and (d) complex viscosity

Figure 9: (a) Schematic representation showing the sampling method from a broken Izod sample and (b) the corresponding TEM image showing the plastic deformation behavior of sample below impact-fractured surface. The representative C8A2E5F2 sample was characterized.

Figure 10: Schematic representation showing the plastic deformation of PLLA component and the orientation of F-CNTs during the impact process. (a) The dispersion of PLLA and F-CNTs in the sample as prepared, (b) PLLA particles act as the stress concentrator, and stress transfer occurs through F-CNTs and (c) the deformation of PLLA particles and the orientation of F-CNTs under

the load condition.

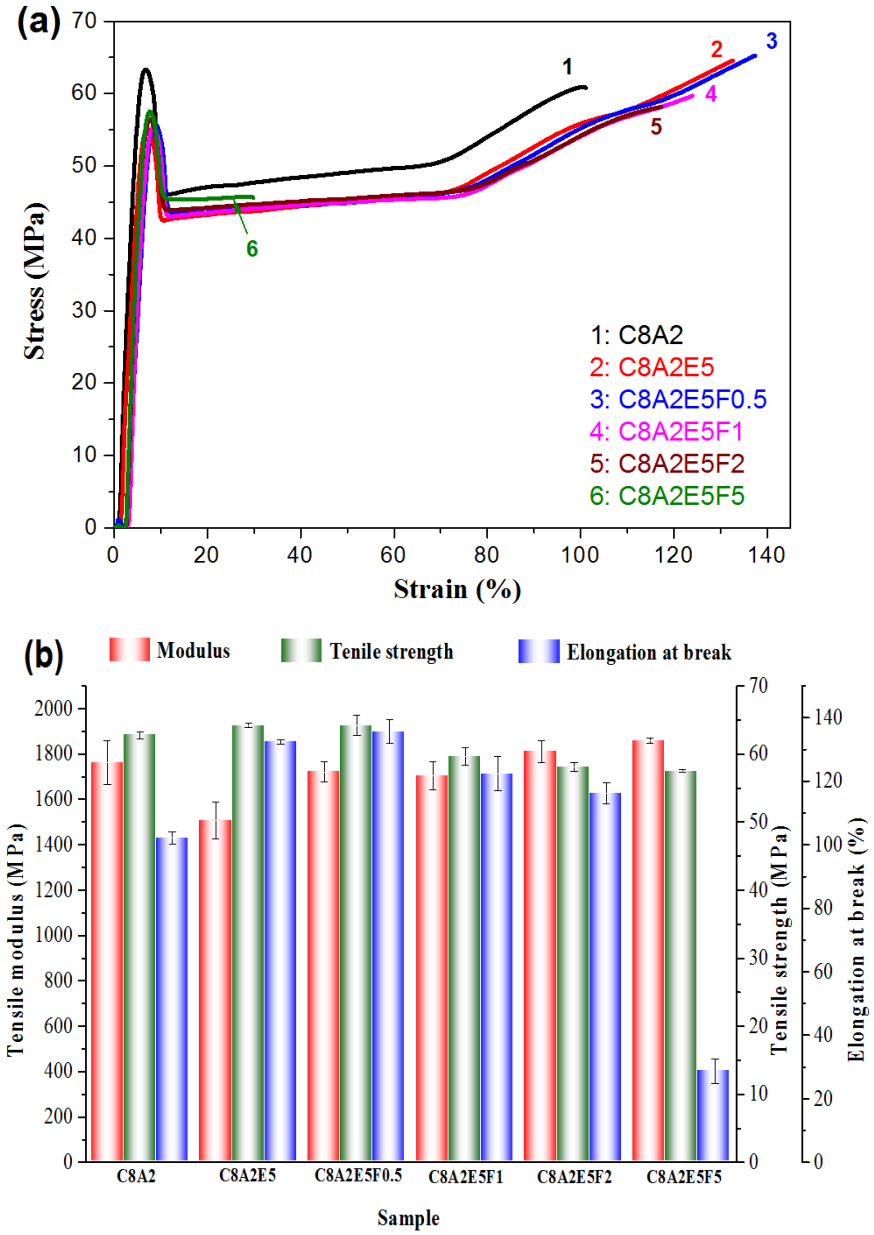

Figure 1

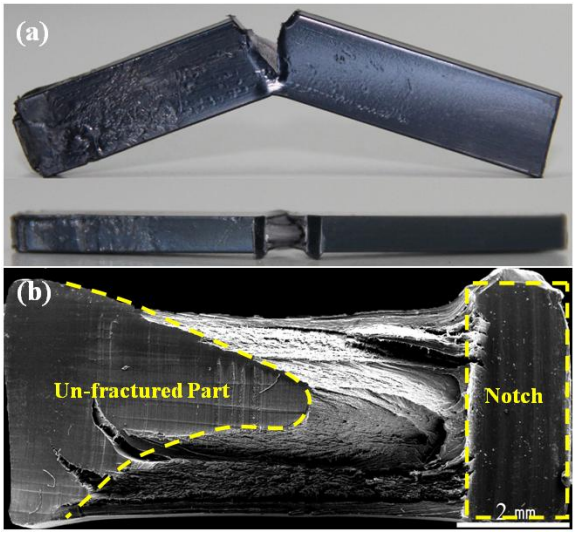

Figure 2

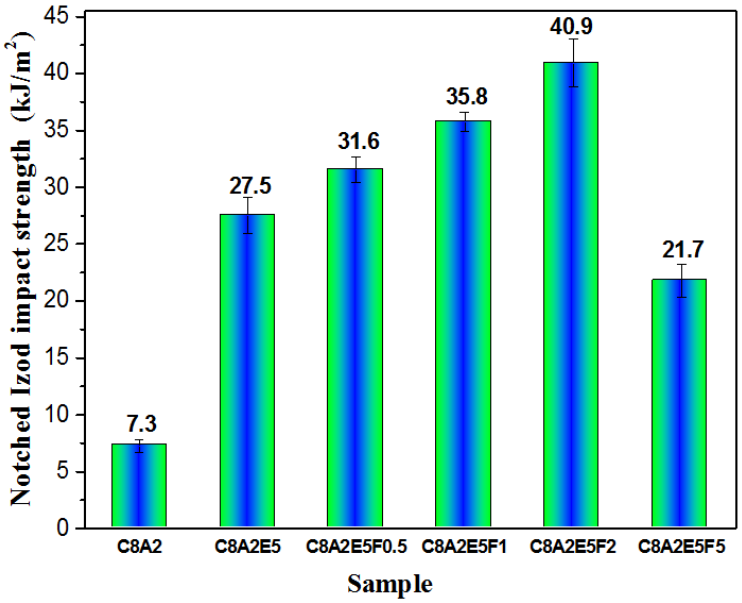

Figure 3

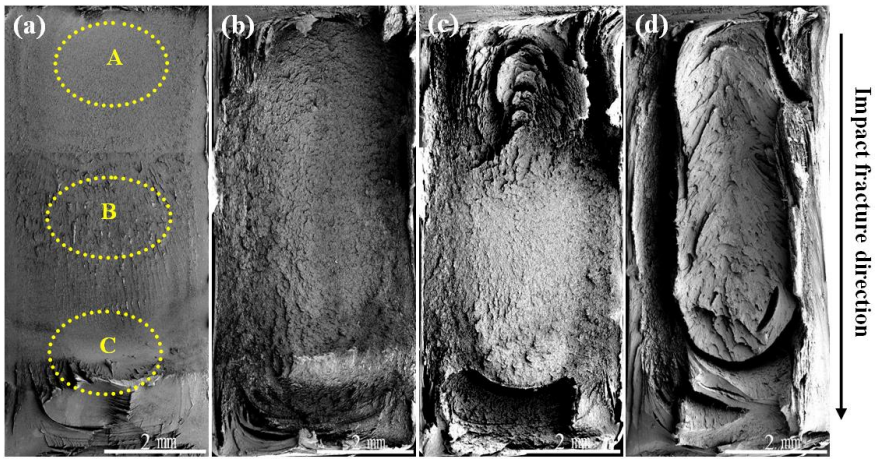

Figure 4

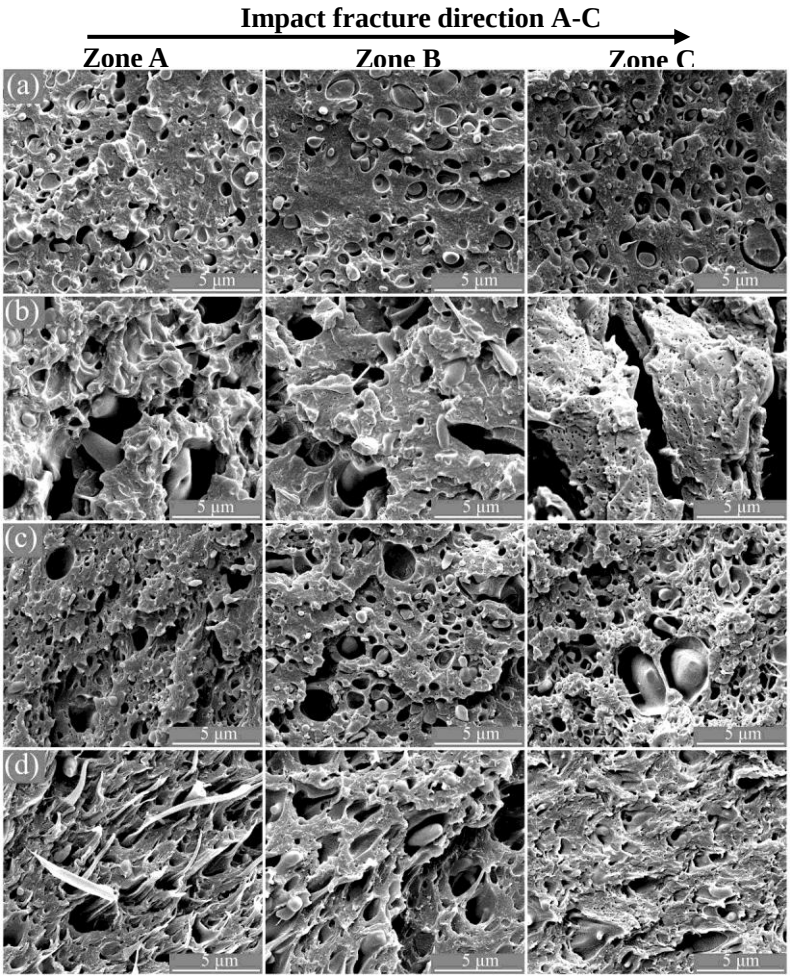

Figure 5

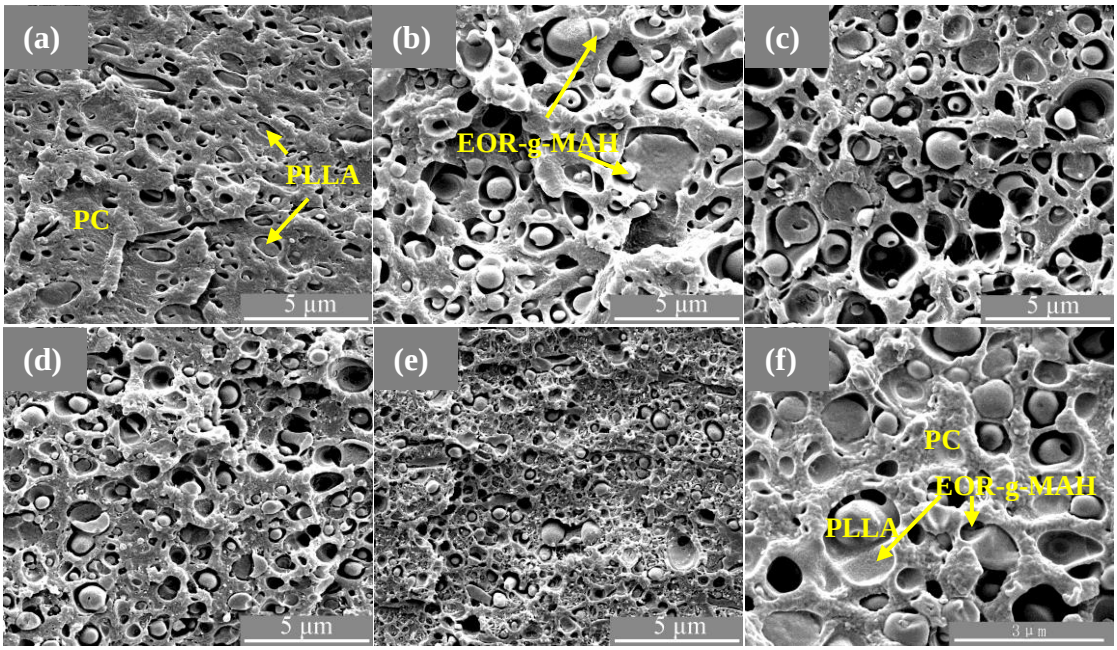

Figure 6

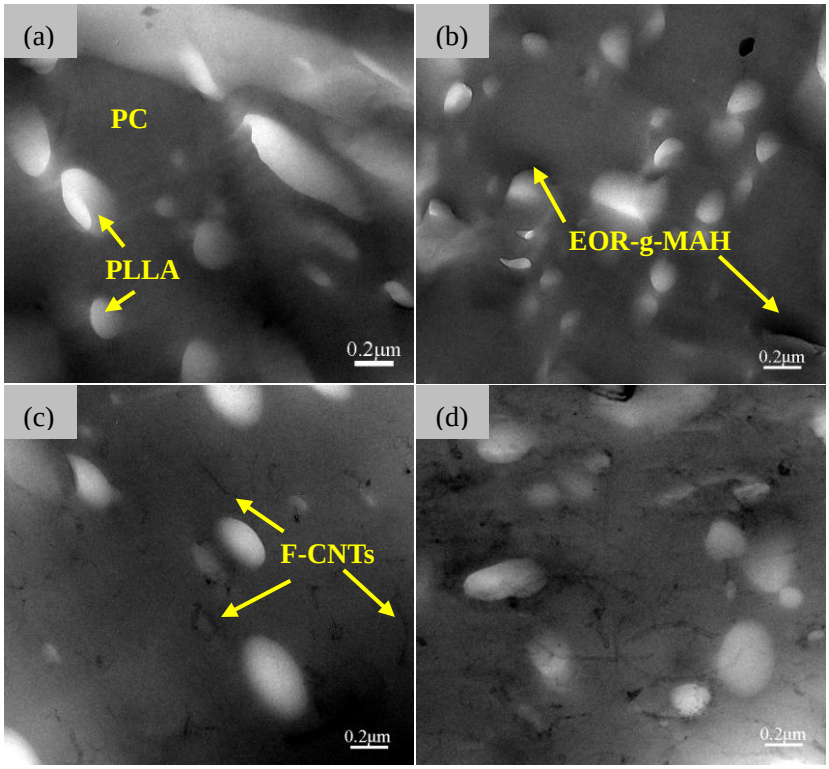

Figure 7

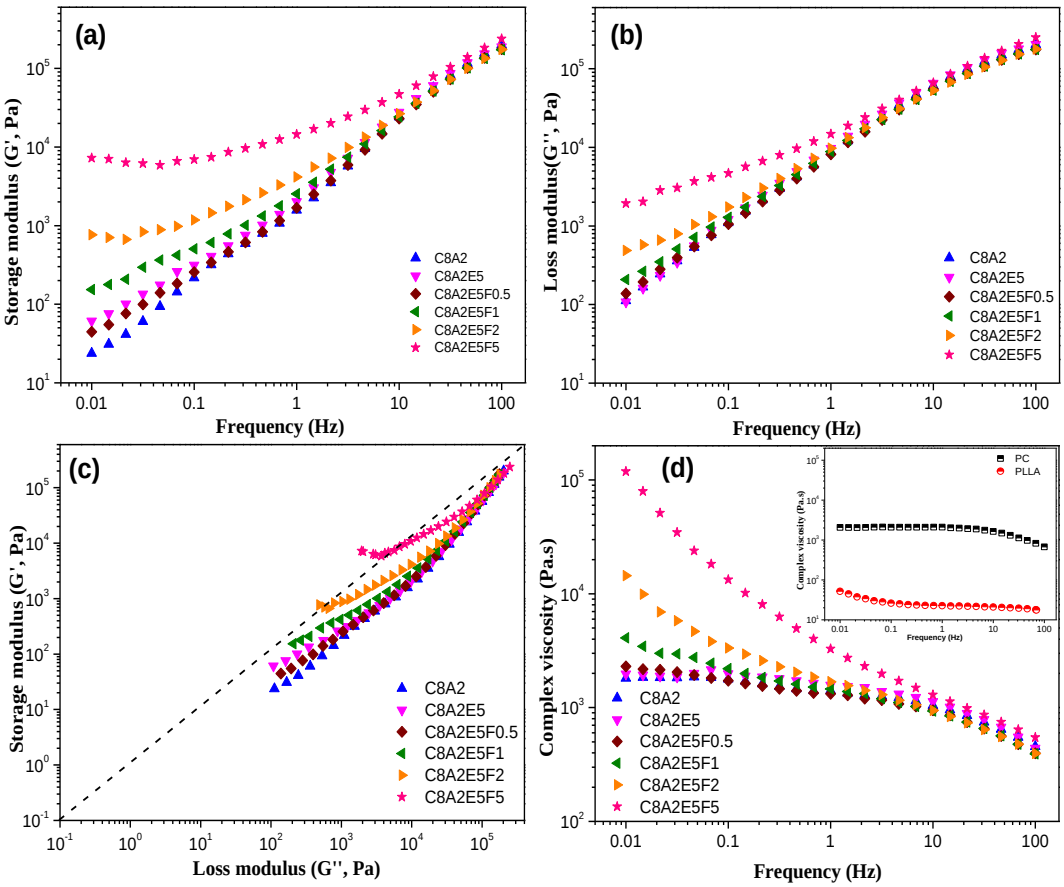

Figure 8

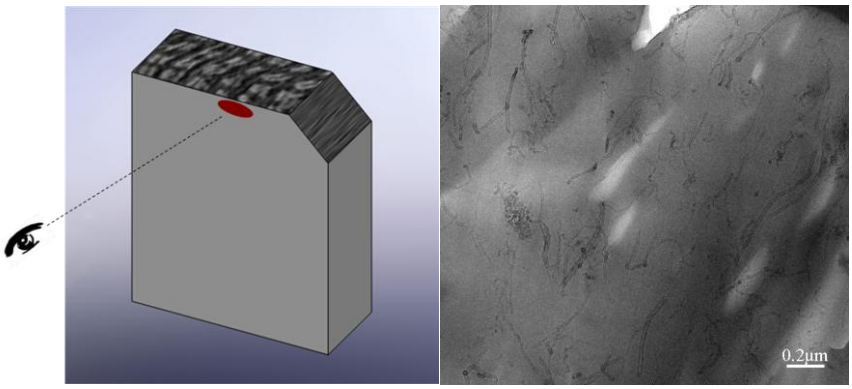

Figure 9

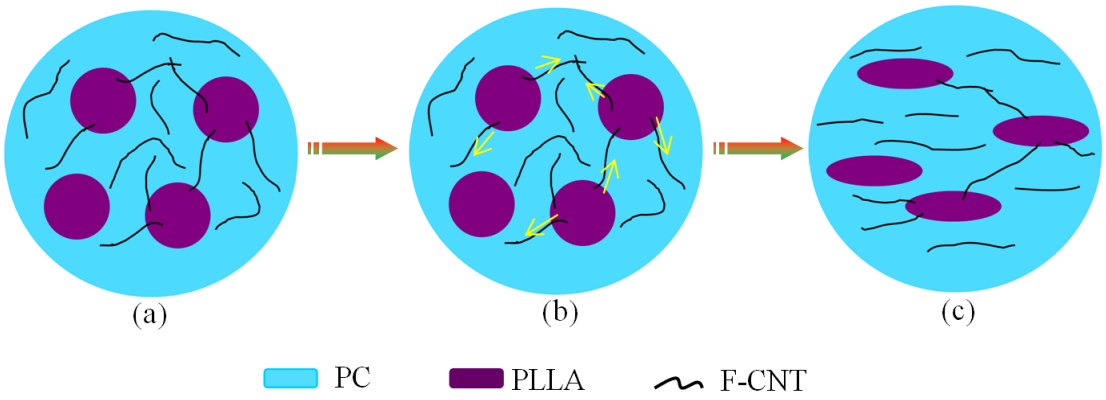

Figure 10

Table of Content use only

Super toughed immiscible polycarbonate/poly(L-lactide) blend achieved by simultaneous addition of compatibilizer and carbon nanotubes

Yong-hong Wang, Xian-ling Xu, Jian Dai, Jing-hui Yang, Ting Huang, Nan Zhang, Yong Wang, Zuo-wan Zhou, Ji-hong Zhang

Key Laboratory of Advanced Technologies of Materials (Ministry of Education), School of Materials Science & Engineering, Southwest Jiaotong University, Chengdu, 610031, China

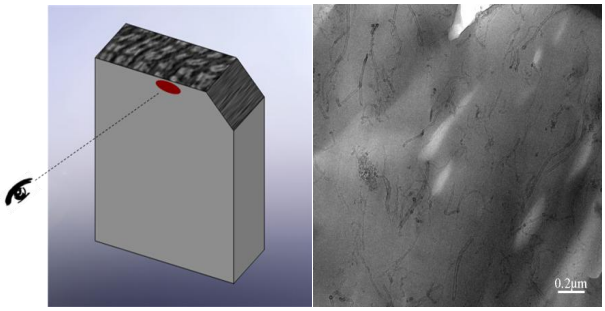

Through improving interfacial interaction and forming CNT network structure, the fracture resistance of immiscible PC/PLLA blend is greatly enhanced.